Residue Specific Resolution of Protein Folding Dynamics Using Isotope-Edited Infrared Temperature Jump Spectroscopy†

Scott H. Brewer,‡ Benben Song,§ Daniel P. Raleigh,*,§ and R. Brian Dyer*,‡

Los Alamos National Laboratory, Chemistry Division, Group PCS, Mail Stop J567, Los Alamos, New Mexico 87545, and State University of New York at Stony Brook, Department of Chemistry, Stony Brook, New York 11794-3400

Received November 15, 2006; Revised Manuscript Received January 16, 2007

ABSTRACT: A major difficulty in experimental studies of protein folding is the lack of nonperturbing, residue specific probes of folding. Here, we demonstrate the ability to resolve protein folding dynamics at the level of a single residue using $^{13}C{=}^{18}O$ isotope-edited infrared spectroscopy. A single $^{13}C{=}^{18}O$ isotopic label was incorporated into the backbone of the 36 residue, three-helix bundle villin headpiece subdomain (HP36). The label was placed in a solvent protected region of the second α-helix of the protein. The $^{13}C{=}^{18}O$ isotopic label shifted the carbonyl stretching frequency to 1572.1 cm^{-1} in the folded state, well removed from the $^{12}C{=}^{16}O$ band of the unlabeled protein backbone. The unique IR signature of the $^{13}C{=}^{18}O$ label was exploited to probe the equilibrium thermal unfolding transition using temperature-dependent FTIR spectroscopy. The folding/unfolding dynamics were monitored using temperature-jump (T-jump) IR spectroscopy. The equilibrium unfolding studies showed conformational changes suggestive of a loss of helical structure in helix 2 prior to the global unfolding of the protein. T-jump relaxation kinetics probing both the labeled site and the $^{12}C{=}^{16}O$ band were found to be biphasic with similar relaxation rates. The slow relaxation phase ($\sim 2 \times 10^5$ s^{-1}) corresponds to the global folding transition. The location of the label, a buried position in helix 2, provides an important probe of the origin of the fast relaxation phase ($\sim 10^7$ s^{-1}). This phase has significant amplitude for the labeled position even though it is well protected from solvent in the folded structure. The fast phase likely represents a rapid pre-equilibrium that involves solvent penetration around the label and possible partial unfolding of helix 2 prior to the global unfolding transition. This work represents the first experimental study of ultrafast folding dynamics with residue specific resolution.

A major difficulty in experimental studies of protein folding, particularly for studies of rapidly folding proteins, is the inability to probe folding dynamics at the level of an individual residue in a nonperturbing fashion. Infrared spectroscopy is an effective method for the study of protein conformational and structural changes on all relevant time scales, and high structural specificity can be achieved by isotope-editing. For instance, nonperturbing isotope labels can be incorporated into the amide carbonyl groups of the peptide backbone. A $^{13}C{=}^{16}O$ label shifts the carbonyl stretching frequency lower in energy than the corresponding $^{12}C{=}^{16}O$ stretching frequency. Single ^{13}C isotopic labels have been used successfully in peptide systems to obtain residue specific information (*1*−*6*). When extended to proteins, however, this approach suffers from overlap with the $^{12}C{=}^{16}O$ band and from the natural abundance of ^{13}C. Since the natural abundance of ^{13}C is about 1.07%, (*7*) this interference becomes significant for larger proteins and can even be a complicating factor for midsized and small proteins. A potential solution to these problems is the use of the nonperturbing $^{13}C{=}^{18}O$ isotopic label. The $^{13}C{=}^{18}O$ isotopic label shifts the carbonyl stretching frequency farther away from the $^{12}C{=}^{16}O$ band, and the low natural abundance (*7*) (0.20%) of ^{18}O gives a probability of 0.002% of having a natural abundance $^{13}C{=}^{18}O$ bond in the protein (*4*, *8*−*10*). The methodology has, however, so far been restricted to peptide systems and has not yet been applied to globular proteins. Here, we test the use of this label for the first time in a protein to follow the equilibrium and kinetics of folding with single residue specificity.

The $^{13}C{=}^{18}O$ labeling will be most useful when the $^{13}C{=}^{18}O$ group does not have any or has only minimal coupling with neighboring $^{12}C{=}^{16}O$ groups. In this case, residue specific information can be obtained. 2D-IR experiments have shown that some coupling does exist between a $^{13}C{=}^{18}O$ oscillator and neighboring $^{13}C{=}^{16}O$ groups, however the larger frequency difference $^{13}C{=}^{18}O$ and $^{12}C{=}^{16}O$ oscillators should decrease this coupling (*4*−*8*). Therefore, the $^{13}C{=}^{18}O$ label should be a probe of local structure, which we verify in this study.

We incorporated a single $^{13}C{=}^{18}O$ label into the peptide backbone of a 36 residue protein, the villin headpiece subdomain (HP36). The villin headpiece subdomain is a three-helix bundle, thermostable protein whose structure is

† This work was funded by NIH Grant GM 53640 to R.B.D., NSF Grant MCB614365 to D.P.R., and a Los Alamos National Laboratory Director's Postdoctoral Fellowship to S.H.B.

* Corresponding authors. R.B.D.: e-mail, bdyer@lanl.gov; phone, (505) 667-4194; fax, (505) 667-0440. D.P.R.: e-mail, draleigh@notes.cc.sunysb.edu; phone, (631) 632-9547; fax, (631) 632-7960.

‡ Los Alamos National Laboratory.

§ State University of New York at Stony Brook.

10.1021/bi602372y CCC: $37.00
Published on Web 02/17/2007

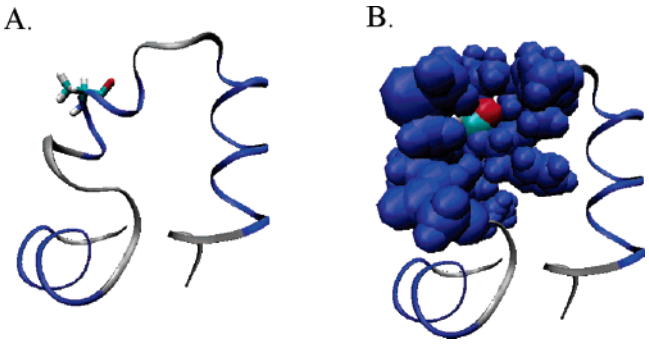

FIGURE 1: Structure of the villin headpiece subdomain (HP36) (Protein Data Bank structure 1VII) highlighting the alanine residue (A57) containing the amide $^{13}C{=}^{18}O$ isotopic label (A). The four residues on either side of A57 are shown in a space-filling representation (blue) to illustrate the solvent accessibility of the carbonyl group of A57 shown in cyan (carbon atom) and red (oxygen atom) (B). The sequence of the protein is MLSDED-FKAVFGMTRSAFANLPLWKQQNLKKEKGLF with A57 in italics. The number of the first residue is 41 using the numbering system from previous publications. The figure was generated using the program VMD (*38*).

shown in Figure 1. This single-domain α-helical protein has been the subject of numerous experimental and computational studies due to its small size and fast folding rate (*11*−*31*). Previously, we observed two distinct relaxation kinetics phases in T-jump[1] IR studies of VHP (*11*). The slower relaxation phase ($\sim 2 \times 10^5$ s^{-1}) was assigned to the global folding/unfolding transition, whereas the faster relaxation phase ($\sim 10^7$ s^{-1}) was assigned to processes occurring within either the folded basin (solvent relaxation) or the unfolded basin (helix−coil relaxation) or both. By strategic placement of the $^{13}C{=}^{18}O$ label at a buried helix position in the protein, we have further explored the origin of the fast relaxation phase. Temperature-dependent difference FTIR spectroscopy was used to probe the thermal unfolding of the $^{13}C{=}^{18}O$ labeled site relative to the rest of the protein. Protein folding dynamics were followed by monitoring both the $^{13}C{=}^{18}O$ stretching mode and the modes due to the unlabeled carbonyl groups using IR T-jump spectroscopy. The results show that a single $^{13}C{=}^{18}O$ label can be selectively detected in a 36 residue protein and that the signal-to-noise is more than sufficient to probe both equilibrium thermal unfolding and time-resolved folding dynamics. Furthermore, the data provide evidence that the fast phase involves a relaxation of helix 2 that occurs at a lower temperature than the global melting of the protein. This study represents the first experimental study of ultrafast folding dynamics with residue specific resolution.

MATERIALS AND METHODS

Sample Preparation. The villin headpiece subdomain (HP36) was prepared by solid-phase peptide synthesis using standard FMOC protocols and purified via reverse phase HPLC. The identity of the purified product was confirmed by mass spectrometry. The C-terminus of the protein was amidated, which does not alter the structure although it slightly reduces the melting temperature. The $^{13}C{=}^{18}O$ label was incorporated into the amide group of alanine 57 according to a previously reported method (*32*) with an isotope incorporation yield of 99% for ^{13}C and 91% for ^{18}O. The numbering system used here corresponds to that of the full length villin headpiece. The first residue in the helical subdomain is Leu-42. Many studies of the headpiece subdomain have made use of recombinant protein which includes an additional Met at the N-terminus. This Met, which is the first residue in the construct used here, is designated as Met-41 for consistency with previously published studies. The protein was lyophilized from D_2O (Cambridge Isotope Laboratories) to allow deuterium−hydrogen exchange of the amide protons to occur. The protein was dissolved in a buffer containing 10 mM sodium phosphate and 150 mM sodium chloride at a pH* of 5.8 in D_2O. pH* refers to the uncorrected (for D_2O) pH-meter reading at 25 °C. The protein solutions were filtered to remove any aggregates present and used without any further purification. The protein solutions for the IR experiments had a concentration of ∼1 mM.

Equilibrium FTIR Temperature-Dependent Measurements. Equilibrium FTIR temperature-dependent spectra were recorded on a Bio-Rad FTS-40A FTIR spectrometer equipped with a liquid nitrogen cooled mercury cadmium telluride (MCT) detector. The spectra were the result of 256 scans recorded at a resolution of 2 cm^{-1}. The proteins were dissolved in D_2O (instead of H_2O) to remove solvent interference in the amide I′ region (the prime indicates that D_2O is the solvent). A split IR cell composed of CaF_2 windows was utilized with a path length of 100 μm to record the spectrum of both the reference (buffer in D_2O) and the sample (protein in the D_2O buffer) side of the IR transmission cell under identical conditions at each temperature. The temperature of the IR cell was controlled by a water bath, and the sample temperature was measured by a thermocouple attached to the cell. The absorbance spectra of the protein were determined from the negative logarithm of the ratio of the single beam spectra of the sample to the reference side of the IR split cell at each temperature. A two-point baseline correction was utilized for the absorbance spectra. The equilibrium thermal unfolding of the protein was found to be reversible (absence of aggregation).

Time-Resolved Temperature-Jump (T-Jump) IR Kinetic Measurements. The time-resolved T-jump apparatus used to measure the protein relaxation kinetics in this study has been described previously (*11*). This method is a pump−probe experiment where 1.91 μm radiation is the pump beam that initiates a rapid T-jump in the sample, thereby perturbing the folding equilibrium. A CW lead salt IR diode laser (Laser Components Instrument Group, Wilmington, MA, tunable in the 1550−1650 cm^{-1} region) is used to probe structural changes in the sample as the system relaxes to a new equilibrium at the final temperature in response to the T-jump. The changes in transmission of the IR probe beam are detected by a fast (200 MHz) photovoltaic (PV) MCT detector (Kolmar Technologies, Newburyport, MA). The 1.91 μm (10 ns fwhm Gaussian pulse width, ∼20 mJ/pulse) pump radiation is obtained from a H_2 filled Raman shifter (1 stokes shift) pumped by a 10 Hz repetition rate Q-switched DCR-4 Nd:YAG laser (Spectra Physics, Mountain View, CA) and is absorbed by weak combination bands in the D_2O solution.

[1] Abbreviations: A57($^{13}C{=}^{18}O$) HP36, the helical subdomain of the villin headpiece (HP36) with a $^{13}C{=}^{18}O$ isotopic label incorporated into the peptide backbone amide group of A57; SASA, solvent accessible surface area; T_m, the midpoint of the thermal unfolding transition; T-jump, temperature-jump.

This pump radiation was chosen due to its transmission properties (87% pump radiation transmitted through 100 μm path length sample cell) that allow for nearly uniform heating in the pump−probe overlap region and because most peptides and proteins do not absorb at this wavelength. The same split cell used for the equilibrium FTIR experiments was used for the kinetic measurements with the reference D_2O buffer compartment serving as an internal thermometer to determine the magnitude of the T-jump. The protein relaxation kinetic traces were extracted by subtracting the change in absorbance of the reference (D_2O buffer) from the sample (protein in D_2O buffer) in response to the T-jump. The kinetic traces were recorded from the nanosecond to tens of milliseconds time regime with the thermal energy diffusing from the pump−probe interaction volume in about 20 ms and were fit to a biexponential function. The data analysis was performed in IGOR Pro (Wavemetrics, Inc.).

RESULTS AND DISCUSSION

Structure of the Villin Headpiece Subdomain. The structure of the villin headpiece subdomain (PDB 1VII) is shown in Figure 1. The villin headpiece subdomain is a three-helix bundle protein consisting of three α-helices that pack to form the hydrophobic core. The sequence of our 36 residue construct (HP36) is MLSDEDFKAVFGMTRS*A*FANLPLWKQQNLKKEKGLF. The first residue is Met41, included because prior studies of recombinant versions of the headpiece helical subdomain included an additional N-terminal Met. This residue is not found in the native intact headpiece. The numbering system used here corresponds to that of the full length villin headpiece. The first residue in the helical subdomain is Leu-42. The NMR structure defines two short helices consisting of residues D44−K48 and R55−F58, respectively with a longer C-terminal helix consisting of residues L63−E72 (*19*). Ala57 in the second helix was chosen as the site for the incorporation of the $^{13}C{=}^{18}O$ label. A57 is denoted in italics in the sequence and is highlighted in the structure in Figure 1. This residue was selected since it is in a predominately buried position in helix 2 and should therefore report on core formation and breakup. Conversely, this position should be relatively insensitive to solvent rearrangements compared to the solvent exposed portions of the native structure. Initially we investigated the use of the simpler $^{13}C{=}^{16}O$ label, however, this label suffered from the background absorbance of the $^{13}C{=}^{16}O$ natural abundance and $^{12}C{=}^{16}O$ stretching bands. Specifically, the ^{13}C label alone shifts the A57 band from 1647 to 1610 cm^{-1}, where it is still partially obscured by the unlabeled amide I′ band.

Temperature-Dependent Equilibrium FTIR Spectroscopy. The FTIR absorbance spectrum of A57($^{13}C{=}^{18}O$) HP36 shows an amide I′ band at 1645 cm^{-1} at 7 °C, which is characteristic of a helical protein (data not shown). The stretching frequency of the $^{13}C{=}^{18}O$ label is shifted lower in energy relative to the unlabeled $^{12}C{=}^{16}O$ backbone and is well resolved, which allows the structure and dynamics of the labeled residue to be probed independently from the bulk. Figure 2 shows the temperature-dependent equilibrium difference FTIR spectra of A57($^{13}C{=}^{18}O$) HP36 from 7 °C to 86 °C in ∼10 °C increments. The difference spectra allow the temperature-dependence of the $^{13}C{=}^{18}O$ stretching mode to be more easily viewed, compared to regular absorbance spectra. The difference spectra are formed by subtracting the lowest temperature absorbance spectrum from the spectra recorded at higher temperatures. The difference spectra show negative features in the range of 1604−1656 cm^{-1} and positive features in the 1656−1740 cm^{-1} range that increase in intensity with increasing temperature. These features are due to the loss of secondary and tertiary structure with a concomitant increase in disordered regions of the protein, respectively. These two regions follow the $^{12}C{=}^{16}O$ groups of the peptide backbone. The decrease in intensity in the 1604−1656 cm^{-1} region is composed primarily of two overlapping bands centered at ∼1632 and ∼1646 cm^{-1} similar to what was observed with unlabeled HP36 (*11*). These two components represent $^{12}C{=}^{16}O$ groups in helices which are on the solvent exposed face ("solvated helix") or are protected from solvent ("buried helix"), respectively. The ∼1632 cm^{-1} component is composed of $^{12}C{=}^{16}O$ oscillators that are hydrogen bonded both to amide groups in the helix and to water molecules of the solvent, while the ∼1646 cm^{-1} component is composed of helical $^{12}C{=}^{16}O$ groups buried in the hydrophobic core (*11*, *33*, *34*). Regions of either decreasing or increasing intensity as a function of increasing temperature appear at 1559−1579 cm^{-1} and 1579−1604 cm^{-1}, respectively in the difference FTIR spectra. These regions probe the $^{13}C{=}^{18}O$ amide stretching mode of A57 as the protein thermally unfolds. The negative feature centered at 1572.1 cm^{-1} follows the loss of secondary and tertiary structure involving A57, while the positive region is indicative of A57 involved in disordered structure.

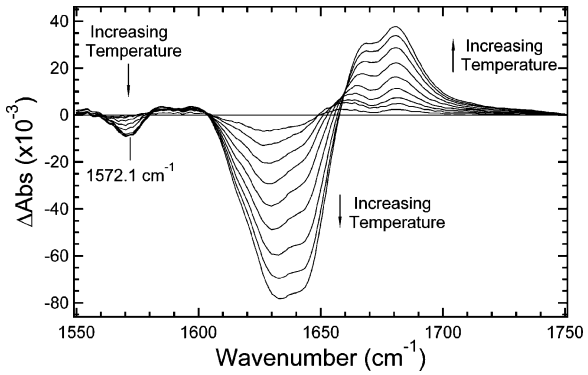

FIGURE 2: Temperature-dependent difference FTIR spectra of A57-($^{13}C{=}^{18}O$) HP36 from 7 °C to 86 °C in ∼10 °C increments. The difference spectra are produced by subtracting the lowest temperature absorbance spectrum from the higher temperature spectra. The peak corresponding to the carbonyl stretch of the $^{13}C{=}^{18}O$ label for residue A57 appears at 1572.1 cm^{-1} in the folded state.

The difference FTIR spectra of A57($^{13}C{=}^{18}O$) HP36 clearly show that a single $^{13}C{=}^{18}O$ isotopic label can be detected in a 36 residue protein. The $^{13}C{=}^{18}O$ stretching mode of A57 in the folded state occurs at 1572.1 cm^{-1} in the temperature-dependent difference FTIR spectra. Measurement of the position of the $^{12}C{=}^{16}O$ stretch for A57 would give insight into whether this carbonyl group is solvent exposed, buried in the hydrophobic core, or in a position in between these two extremes (*11*, *33*−*36*). The unlabeled stretching frequency can be determined by subtracting the FTIR absorbance spectrum of A57($^{13}C{=}^{18}O$) HP36 from the WT HP36 absorbance spectrum. Figure 3 shows that the resulting difference spectrum at 25 °C contains two prominent peaks. The high level of ^{13}C (99%) and ^{18}O (91%) incorporation into the A57 site produces a clean difference

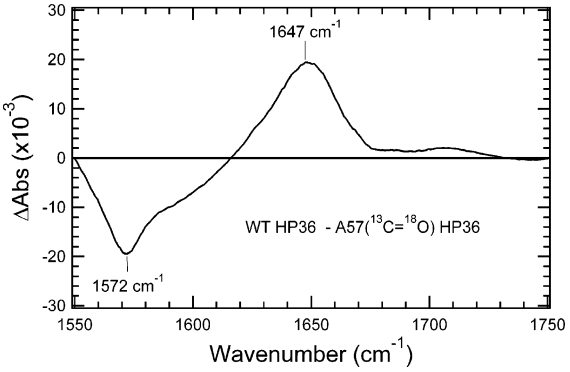

FIGURE 3: The difference spectrum produced by subtracting the absorbance spectrum of A57($^{13}C{=}^{18}O$) HP36 (pH* 5.8) from the absorbance spectrum of wild type HP36 (pH* 5.3) at 25 °C. The modes at 1572 and 1647 cm^{-1} are due to the $^{13}C{=}^{18}O$ and $^{12}C{=}^{16}O$ carbonyl stretching frequencies of A57, respectively. The minor spectral features at 1594 and 1704 cm^{-1} are due to the slight pH* mismatch between the two samples.

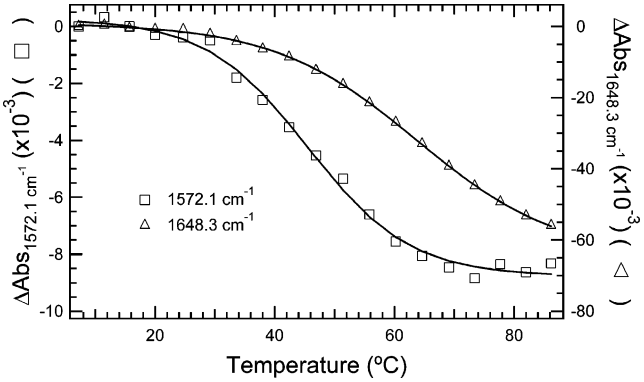

FIGURE 4: Thermal unfolding transition of A57($^{13}C{=}^{18}O$) HP36 monitored at 1572.1 cm^{-1} (squares) and 1648.3 cm^{-1} (triangles). The solid curves are the best fit to a two-state unfolding transition.

spectrum with only two major peaks. The negative peak at 1572 cm^{-1} is due to the $^{13}C{=}^{18}O$ stretching frequency, and the positive peak at 1647 cm^{-1} is due to the carbonyl stretching frequency of A57 in the unlabeled protein. Two other minor peaks appear at 1594 and 1704 cm^{-1} in the difference spectrum. These modes are due to the slight pH* mismatch of the two samples (pH* 5.3 vs pH* 5.8) resulting in a difference in the relative population of protonated vs unprotonated carboxylate groups in amino acid side chains. The $^{12}C{=}^{16}O$ stretching frequency of a completely buried carbonyl group in an α-helical protein have been shown to be ~1652 cm^{-1} while the band due to a solvent exposed carbonyl group in a helix is found at ~1632 cm^{-1}, respectively (*34*). Therefore, the position of the unlabeled carbonyl group of A57 in this protein suggests that this carbonyl group is primarily in a buried site with little interaction with D_2O. This result is confirmed by solvent accessible surface area (SASA) calculations using the software GETAREA (*37*) (version 1.1). The SASA for the carbonyl group (sum of the SASA for the carbon and oxygen atom of the carbonyl group) for A57 is 2.1 $Å^2$ using a probe radius of 1.4 Å. This value is close to the SASA value of the carbonyl group of the completely buried hydrophobic core residue F47 (0.0 $Å^2$). For comparison, the SASA of the carbonyl group of the solvent exposed residue A49 is 19.2 $Å^2$.

The observed isotope shift is consistent with a localized (weakly coupled) C═O stretch for A57. If the C═O stretch of A57 is treated as a local oscillator, the expected isotopic shift between $^{13}C{=}^{18}O$ and $^{12}C{=}^{16}O$ is 77 cm^{-1} based upon the difference in reduced mass of the two carbonyl groups. The experimental and calculated isotopic shifts of the $^{13}C{=}^{18}O$ group differ by only 2 cm^{-1}, consistent with weak coupling between A57 ($^{13}C{=}^{18}O$) and other carbonyl groups in the protein. The similar intensities of the two bands in the difference spectrum are also evidence of weak coupling. While strong coupling has been observed in other helical systems, (*4*) the weak coupling observed in this case likely results from the short length of helix 2 (a single turn) and the large isotope shift of the double label which effectively isolates this vibration. Consequently, we interpret the A57 ($^{13}C{=}^{18}O$) stretch as a local mode that reports on the specific structure and dynamics of this residue and its immediate contacts.

The unfolding of the A57($^{13}C{=}^{18}O$) HP36 protein can be followed either globally in the amide I′ region by following the unlabeled $^{12}C{=}^{16}O$ stretching modes or locally using the $^{13}C{=}^{18}O$ stretching mode of A57. Figure 4 shows the melting profile at 1648.3 cm^{-1} ($^{12}C{=}^{16}O$, triangles) and at 1572.1 cm^{-1} ($^{13}C{=}^{18}O$, squares). The former frequency probes the disruption of the hydrophobic core upon unfolding, while the latter monitors local conformational changes of the $^{13}C{=}^{18}O$ group of A57. The two temperature profiles are clearly different with the 1572.1 cm^{-1} thermal unfolding transition having a lower T_m (midpoint of the thermal unfolding transition) relative to the melting profile at 1648.3 cm^{-1}. The difference in the melting behavior of the labeled and unlabeled carbonyl groups was confirmed through a singular value decomposition analysis of the temperature-dependent FTIR spectra in Figure 2. The 1572.1 cm^{-1} melt curve begins to level off at higher temperatures and displays a well-defined post-transition baseline, unlike the 1648.3 cm^{-1} thermal profile. Individual fits to the melt curves yield a T_m of 63.7 °C at 1648.3 cm^{-1}, while the 1572.1 cm^{-1} melt curve gives a T_m of 45.5 °C. The lack of an isosbestic point in the temperature-dependent difference FTIR spectra (Figure 2) of this protein also suggests the presence of more than one thermal unfolding transition. A quantitative thermodynamic analysis of the melt would clearly require at least 3-states to account for this behavior; however, such an analysis is beyond the scope of this paper. The 1648.3 cm^{-1} melt transition follows the sum of the conformation changes of the $^{12}C{=}^{16}O$ oscillators primarily in the hydrophobic core upon unfolding and consequently reports on the global unfolding of the protein. The 1572.1 cm^{-1} thermal profile, however, gives site-specific information on the temperature-induced conformation changes of the labeled carbonyl group of residue 57. The lower transition temperature for the A57 site could be due to the partial or complete melting of structure near A57 prior to complete global unfolding of the protein. Temperature-dependent changes in solvation and hydrogen bonding of the $^{13}C{=}^{18}O$ group of A57 with the aqueous solvent might also contribute. Such effects could result directly from conformational changes at A57 or from side-chain conformational changes of neighboring residues that shielded the $^{13}C{=}^{18}O$ group in the low-temperature structure.

Time-Resolved IR Temperature-Jump Spectroscopy. We have followed the local folding and unfolding dynamics of A57($^{13}C{=}^{18}O$) HP36 using T-jump IR spectroscopy. Figure

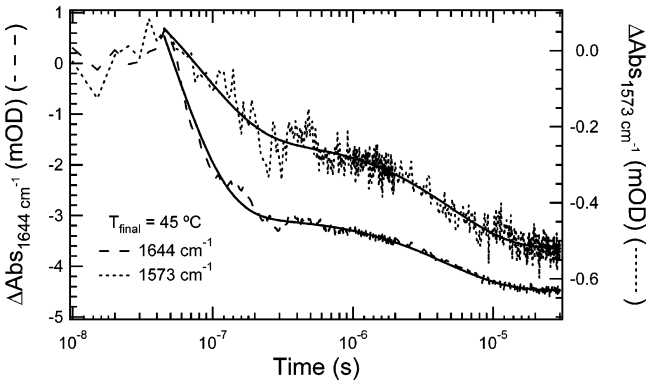

FIGURE 5: Temperature-jump relaxation kinetics monitored at 1573 cm^{-1} (short dashed) and 1644 cm^{-1} (long dashed) for A57($^{13}C{=}^{18}O$) HP36 in response to a T-jump from 41 °C to 45 °C. The kinetic traces at 1573 and 1644 cm^{-1} are the result of 16 000 or 10 000 laser shots, respectively. The kinetic traces are fit with a biexponential function (solid curves).

5 shows the T-Jump IR relaxation kinetics monitored both at 1573 cm^{-1} (short dashed trace) that probes the $^{13}C{=}^{18}O$ isotopic label and at 1644 cm^{-1} (long dashed trace) that follows the $^{12}C{=}^{16}O$ amide carbonyl groups. The magnitude of the T-jump was 4 °C for both probe frequencies with a final temperature of 45 °C. Both transients exhibit biphasic relaxation kinetics and can be fit to biexponential functions (solid traces). The observed relaxation rates derived from the double exponential fits of the transient at 1573 cm^{-1} are 1.23×10^7 s^{-1} and 1.99×10^5 s^{-1} compared to 2.14×10^7 s^{-1} and 2.16×10^5 s^{-1} for the fit to the 1644 cm^{-1} transient. The kinetic transient at 1644 cm^{-1} includes contributions from both buried and solvated helix components due to the overlap of the components at this frequency. Previous IR and fluorescence T-jump studies of the villin headpiece subdomain also showed biphasic relaxation kinetics (*11*, *12*). The slow (microsecond) process reports on the global folding and unfolding of the protein (the rate-limiting step of crossing the main barrier to folding), while the fast kinetic process is likely due to relaxation in either the folded or the unfolded free energy basin, or both. The fast relaxation rate is on a time scale consistent with the re-equilibration of the helix−coil transition (a characteristic rate observed for both model peptides and other helical proteins), probably including solvent rearrangement around the helices, in response to the temperature change. The presence of two kinetic phases along with the multiple transitions observed in the temperature-dependent difference FTIR spectra can be accounted for by relaxation of the protein in the folded and/or unfolded free energy basins of the protein. The similarity in observed microsecond relaxation times measured at both wavelengths is expected for the folding of a protein with one dominant activation energetic barrier along the folding pathway.

The relative amplitude of the fast phase is smaller for the 1573 cm^{-1} transient compared to the 1644 cm^{-1} transient. If the fast phase were solely due to the solvated helix relaxation, its amplitude should be greater at 1644 cm^{-1}, since this frequency has a significant contribution from the solvated helix band. Significant amplitude is observed for the fast phase of the transient monitored at 1573 cm^{-1}, however, despite the position of the $^{13}C{=}^{18}O$ label in a predominantly buried site in the native structure. The equilibrium melt curves (Figure 4) provide some insight on the origin of the fast phase observed at 1573 cm^{-1}. The final temperature of the T-jump (45 °C) is near the T_m of the unfolding transition monitored at the labeled position, which is considerably lower than the global melt monitored at the unlabeled amide I band. Temperature-induced A57 conformational changes might decrease the structural integrity of helix 2, resulting in the observation of the helix−coil equilibrium at this final T-jump temperature. Alternatively, conformational changes either in A57 or in the side-chains of neighboring residues that shield the labeled group from solvent might occur resulting in increased hydration of A57. This increased hydration would result in an increase in the amplitude of a fast phase caused by temperature-induced solvent reorganization around the protein such as solvent hydrogen bonding to the $^{13}C{=}^{18}O$ group. Regardless of which mechanism predominates, the equilibrium and kinetic measurements of the A57 $^{13}C{=}^{18}O$ group both suggest a complex folding mechanism that is not strictly two-state. Both measurements are consistent with a temperature-induced change in environment of the $^{13}C{=}^{18}O$ group resulting in a more solvent-exposed residue and a loss of local structure probed at A57 prior to the global unfolding of the protein. Isotope-edited experiments involving additional sites could yield further insight into whether the fast observed relaxation phase is due to relaxation in the folded basin or has contributions from relaxation of residual helical structure in the unfolded basin. Along these lines it is worth noting that previous studies have provided indirect evidence for significant structure in the unfolded state of HP36 including partial helical structure involving the two short N-terminal helices.

CONCLUSIONS

The results presented here demonstrate for the first time the ability of isotope-edited infrared spectroscopy to provide single residue specificity in equilibrium and kinetics measurements of protein folding. Since an isotope label can be incorporated selectively and without perturbing the structure or the dynamics, it offers the ultimate noninvasive probe of folding dynamics. Furthermore, isotope-editing is a completely general method since single $^{13}C{=}^{18}O$ isotopic labels can be readily incorporated into small to midsize proteins using standard solid-phase peptide synthesis protocols. Labels can be incorporated into larger domains using either peptide ligation methods or expressed protein ligation. In comparison, NMR relaxation is the only competitive technique that can yield site specific information about folding kinetics without the addition of perturbing labels. The NMR method, while very powerful, does suffer from the limitation that it is conducted at equilibrium. It can be experimentally difficult to fit protein NMR relaxation data to multistage transitions. In addition, the NMR relaxation method requires a unique resonance that by chance is well isolated from any other interfering peaks over the entire range of the folding transition. Generally only one such resonance can be found for a given protein, if any at all. Larger proteins are not usually accessible to this approach, due to the increase in spectral congestion. In contrast, the isotope-edited infrared approach does not share any of these limitations. First, the T-jump relaxation method directly probes folding kinetics in real time, so that complex kinetics are resolved directly. Second, the number of available probes is only limited by the synthetic difficulties of incorporating the isotopic labels,

so that in principle almost any backbone position can be labeled. Commercially available amino acids with the $^{13}C{=}O$ label include Ala, Gln, Glu, Gly, Ile, Leu, Lys, Met, Phe, Ser, and Val, and others are available through custom synthesis. Finally, the technique is not limited by the number of amino acids in the protein since the isotope shift and hence the resolution of the labeled peak are independent of protein size.

In the present study, a single $^{13}C{=}^{18}O$ isotopic label was sufficient to probe the equilibrium unfolding and the folding kinetics of HP36 with high selectivity and high sensitivity. The results provide new insight into the folding of this model helical protein. The observation of a distinct thermal unfolding transition for the A57 site reveals the surprising complexity of the folding of this protein despite its small size and simple topology. This separate transition cannot be detected by conventional CD, fluorescence, or IR monitored unfolding studies. The unique melting behavior of the labeled structure is correlated with significant amplitude of a fast phase in the T-jump kinetics. This fast phase is attributed to the increase in solvent accessibility of the A57 site at the final temperature of the T-jump. Thus, the fast phase likely represents a rapid pre-equilibrium that involves solvent penetration around the label and possible partial unfolding of helix 2 prior to the global unfolding transition.

ACKNOWLEDGMENT

We thank Dr. Yuefang Tang and Ms. Lauren Wickstrom for helpful discussions.

REFERENCES

1. Decatur, S. M. (2000) IR spectroscopy of isotope-labeled helical peptides: Probing the effect of N-acetylation on helix stability, *Biopolymers 54*, 180−185.
2. Werner, J. H., Dyer, R. B., Fesinmeyer, R. M., and Andersen, N. H. (2002) Dynamics of the primary processes of protein folding: Helix nucleation, *J. Phys. Chem. B 106*, 487−494.
3. Huang, C. Y., Getahun, Z., Zhu, Y. J., Klemke, J. W., DeGrado, W. F., and Gai, F. (2002) Helix formation via conformation diffusion search, *Proc. Natl. Acad. Sci. U.S.A. 99*, 2788−2793.
4. Fang, C., Wang, J., Kim, Y. S., Charnley, A. K., Barber-Armstrong, W., Smith, A. B., III, Decatur, S. M., and Hochstrasser, R. M. (2004) Two-dimensional infrared spectroscopy of isotopomers of an alanine rich alpha-helix, *J. Phys. Chem. B 108*, 10415−10427.
5. Huang, R., Kubelka, J., Barber-Armstrong, W., Silva, R. A. G. D., Decatur, S. M., and Keiderling, T. A. (2004) Nature of vibrational coupling in helical peptides: An isotopic labeling study, *J. Am. Chem. Soc. 126*, 2346−2354.
6. Starzyk, A., Barber-Armstrong, W., Sridharan, M., and Decatur, S. M. (2005) Spectroscopic evidence for backbone desolvation of helical peptides by 2,2,2-trifluoroethanol: An isotope-edited FTIR study, *Biochemistry 44*, 369−376.
7. Rosman, K. J. R., and Taylor, P. D. P. (1998) Isotopic compositions of the elements 1997, *Pure Appl. Chem. 70*, 217−235.
8. Fang, C., Wang, J., Charnley, A. K., Barber-Armstrong, W., Smith, A. B., Decatur, S. M., and Hochstrasser, R. M. (2003) Two-dimensional infrared measurements of the coupling between amide modes of an alpha-helix, *Chem. Phys. Lett. 382*, 586−592.
9. Torres, J., Briggs, J. A. G., and Arkin, I. T. (2002) Multiple site-specific infrared dichroism of CD3-ζ, a transmembrane helix bundle, *J. Mol. Biol. 316*, 365−374.
10. Mukherjee, P., Krummel, A. T., Fulmer, E. C., Kass, I., Arkin, I. T., and Zanni, M. T. (2004) Site-specific vibrational dynamics of the CD3 zeta membrane peptide using heterodyned two-dimensional infrared photon echo spectroscopy, *J. Chem. Phys. 120*, 10215−10224.
11. Brewer, S. H., Vu, D. M., Tang, Y. F., Li, Y., Franzen, S., Raleigh, D. P., and Dyer, R. B. (2005) Effect of modulating unfolded state structure on the folding kinetics of the villin headpiece subdomain, *Proc. Natl. Acad. Sci. U.S.A. 102*, 16662−16667.
12. Kubelka, J., Eaton, W. A., and Hofrichter, J. (2003) Experimental tests of villin subdomain folding simulations, *J. Mol. Biol. 329*, 625−630.
13. Kubelka, J., Chiu, T. K., Davies, D. R., Eaton, W. A., and Hofrichter, J. (2006) Sub-microsecond protein folding, *J. Mol. Biol. 359*, 546−553.
14. Buscaglia, M., Kubelka, J., Eaton, W. A., and Hofrichter, J. (2005) Determination of ultrafast protein folding rates from loop formation dynamics, *J. Mol. Biol. 347*, 657−664.
15. Chiu, T. K., Kubelka, J., Herbst-Irmer, R., Eaton, W. A., Hofrichter, J., and Davies, D. R. (2005) High-resolution X-ray crystal structures of the villin headpiece subdomain, an ultrafast folding protein, *Proc. Natl. Acad. Sci. U.S.A. 102*, 7517−7522.
16. Tang, Y. F., Goger, M. J., and Raleigh, D. P. (2006) NMR characterization of a peptide model provides evidence for significant structure in the unfolded state of the villin headpiece helical subdomain, *Biochemistry 45*, 6940−6946.
17. Tang, Y. F., Rigotti, D. J., Fairman, R., and Raleigh, D. P. (2004) Peptide models provide evidence for significant structure in the denatured state of a rapidly folding protein: The villin headpiece subdomain, *Biochemistry 43*, 3264−3272.
18. Wang, M. H., Tang, Y. F., Sato, S. S., Vugmeyster, L., McKnight, C. J., and Raleigh, D. P. (2003) Dynamic NMR line-shape analysis demonstrates that the villin headpiece subdomain folds on the microsecond time scale, *J. Am. Chem. Soc. 125*, 6032−6033.
19. McKnight, C. J., Matsudaira, P. T., and Kim, P. S. (1997) NMR structure of the 35-residue villin headpiece subdomain, *Nat. Struct. Biol. 4*, 180−184.
20. Vardar, D., Buckley, D. A., Frank, B. S., and McKnight, C. J. (1999) NMR structure of an F-actin-binding "headpiece" motif from villin, *J. Mol. Biol. 294*, 1299−1310.
21. Havlin, R. H., and Tycko, R. (2005) Probing site-specific conformational distributions in protein folding with solid-state NMR, *Proc. Natl. Acad. Sci. U.S.A. 102*, 3284−9.
22. Duan, Y., and Kollman, P. A. (1998) Pathways to a protein folding intermediate observed in a 1-microsecond simulation in aqueous solution, *Science 282*, 740−744.
23. Duan, Y., Wang, L., and Kollman, P. A. (1998) The early stage of folding of villin headpiece subdomain observed in a 200-nanosecond fully solvated molecular dynamics simulation, *Proc. Natl. Acad. Sci. U.S.A. 95*, 9897−9902.
24. Zagrovic, B., Snow, C. D., Shirts, M. R., and Pande, V. S. (2002) Simulation of folding of a small alpha-helical protein in atomistic detail using worldwide-distributed computing, *J. Mol. Biol. 323*, 927−937.
25. Ripoll, D. R., Vila, J. A., and Scheraga, H. A. (2004) Folding of the villin headpiece subdomain from random structures. Analysis of the charge distribution as a function of pH, *J. Mol. Biol. 339*, 915−925.
26. Sanjoy, B., Sudip, C., Balasubramanian, S., Pal, S., and Bagchi, B. (2004) Atomistic simulation study of the coupled motion of amino acid residues and water molecules around protein HP-36: fluctuations at and around the active sites, *J. Phys. Chem. B 108*, 12608−12616.
27. Islam, S. A., Karplus, M., and Weaver, D. L. (2002) Application of the diffusion-collision model to the folding of three-helix bundle proteins, *J. Mol. Biol. 318*, 199−215.
28. Sullivan, D. C., and Kuntz, I. D. (2002) Protein folding as biased conformational diffusion, *J. Phys. Chem. B 106*, 3255−3262.
29. van der Spoel, D., and Lindahl, E. (2003) Brute-force molecular dynamics simulations of villin headpiece: Comparison with NMR parameters, *J. Phys. Chem. B 107*, 11178−11187.
30. Fernandez, A., Shen, M. Y., Colubri, A., Sosnick, T. R., Berry, R. S., and Freed, K. F. (2003) Large-scale context in protein folding: Villin headpiece, *Biochemistry 42*, 664−671.
31. De Mori, G. M. S., Colombo, G., and Micheletti, C. (2005) Study of the villin headpiece folding dynamics by combining coarse-grained Monte Carlo evolution and all-atom molecular dynamics, *Proteins: Struct., Funct., Bioinf. 58*, 459−471.
32. Torres, J., Adams, P. D., and Arkin, I. T. (2000) Use of a new label, $^{13}C{=}^{18}O$, in the determination of a structural model of phospholamban in a lipid bilayer. Spatial restraints resolve the ambiguity arising from interpretations of mutagenesis data, *J. Mol. Biol. 300*, 677−685.
33. Manas, E. S., Getahun, Z., Wright, W. W., DeGrado, W. F., and Vanderkooi, J. M. (2000) Infrared spectra of amide groups in

alpha-helical proteins: Evidence for hydrogen bonding between helices and water, *J. Am. Chem. Soc. 122*, 9883−9890.
34. Vu, D. M., Myers, J. K., Oas, T. G., and Dyer, R. B. (2004) Probing the folding and unfolding dynamics of secondary and tertiary structres in a three-helix bundle protein, *Biochemistry 43*, 3582−3589.
35. Walsh, S. T. R., Cheng, R. P., Wright, W. W., Alonso, D. O. V., Daggett, V., Vanderkooi, J. M., and DeGrado, W. F. (2003) The hydration of amides in helices; a comprehensive picture from molecular dynamics, IR, and NMR, *Protein Sci. 12*, 520−531.
36. Zhu, Y., Alonso, D. O. V., Maki, K., Huang, C. Y., Lahr, S. J., Daggett, V., Roder, H., DeGrado, W. F., and Gai, F. (2003) Ultrafast folding of α_3D: A de novo designed three-helix bundle protein, *Proc. Natl. Acad. Sci. U.S.A. 100*, 15486−15491.
37. Fraczkiewicz, R., and Braun, W. (1998) Exact and efficient analytical calculation of the accessible surface areas and their gradients for macromolecules, *J. Comput. Chem. 19*, 319−333.
38. Humphrey, W., Dalke, A., and Schulten, K. (1996) VMD: Visual molecular dynamics, *J. Mol. Graphics 14*, 33−38.

BI602372Y